Theses and Dissertations

12-14-2015

Confluence of Density Currents Over an Erodible Bed

Hassan Ismail

University of South Carolina - Columbia

Confluence of Density Currents Over an Erodible Bed

by

Hassan Ismail

Bachelor of Science
University of South Carolina 2011

_____

Submitted in Partial Fulfillment of the Requirements

for the Degree of Master of Science in

Civil Engineering

College of Engineering and Computing

University of South Carolina

2015

Accepted by:

Jasim Imran, Director of Thesis

Enrica Viparelli, Reader

M. Hanif Chaudhry, Reader

Lacy Ford, Senior Vice Provost and Dean of Graduate Studies

Dedication

For Heather.

ABSTRACT

Results from laboratory experiments on conservative density current confluence are reported. Hydraulic characteristics and morphodynamic consequences of the confluence of two continuous release density currents in a horizontal, 45° asymmetrical junction are examined and compared to those of terrestrial river junctions. It was observed that density current confluence is markedly different than those in river junctions primarily due to the ease of the dense fluid to convect into the ambient fluid in the junction zone. Upward convection in the junction resulted in low horizontal velocity and shear stresses on the bed of the junction zone, followed by re-plunging to the layer of neutral buoyancy downstream of the junction where acceleration occurs. In the downstream reach was a distinctive erosional pattern similar to central scouring seen in river junctions but starting at the downstream junction point rather than at the upstream junction point. It was found that terrestrial river models match well with the density current case in terms of maximum velocity downstream of the junction, backwater effect, avalanche face protrusion into the downstream reach, and maximum scour orientation. Poor matching was found in terms of separation zone dimensions and shape, streamline deviation angle on the junction line, and maximum scour depth.

TABLE OF CONTENTS

LIST OF FIGURES

Chapter 1

Introduction

Density currents are flows driven by the density difference between a current and ambient fluid (Benjamin 1968). This density difference may be caused by a conservative substance such as dissolved salt, or by a non-conservative substance such as suspended sediment. In particular, turbidity currents are sediment-laden underflows that may travel for very long distances on the ocean floor. They can create self-forming canyons and channels passing over the continental slope and into the abyssal plane (Peakall, McCaffrey, and Kneller 2000). After the slope break at the toe of the continental slope, turbidity currents can deposit their suspended sediments in submarine fans.

Natural turbidity currents are episodic events that, depending on the triggering mechanism and conditions, can be either sustained, quasi-steady flows or surge-type events (Hay 1987). The episodic nature of turbidity currents has left only a few notable instances of direct field observation of turbidity current flows (e.g., Prior et al. 1987; Normark 1989; Khripounoff et al. 2003; Paull et al. 2002; Xu, Noble, and Rosenfeld 2004; Vangriesheim, Khripounoff, and Crassous 2009).

Although a great deal of attention has been placed on the study of submarine channel systems, previous studies have focused heavily on the hydraulics and morphodynamics of individual channels and sinuous submarine channels (e.g., Keeulegan 1949; Simpson and Britter 1979; Parker, Fukushima, and Pantin 1986; Parker et al. 1987; Garcia and Parker 1993; Kneller, Bennett, and McCaffrey 1999; Peakall, McCaffrey, and Kneller 2000; Kneller and Buckee 2000; Peakall et al. 2007; Huang,

Imran, and Pirmez 2008; Islam and Imran 2008; Sequeiros et al. 2010; Huang, Imran, and Pirmez 2012; Ezz, Cantelli, and Imran 2013; Janocko et al. 2013; Tokyay and Garcia 2013). Although submarine channel networks and confluences are well documented through field observation (Canals, Urgeles, and Calafat 2000; Dalla Valle and Gamberi 2011; Greene, Maher, and Paull 2002; Hesse 1989; L'Heureux, Hansen, and Longva 2009; Mitchell 2004; Paquet et al. 2010; Straub et al. 2011, e.g.,), little attention has been placed on understanding the characteristics and physical processes of these settings.

Hesse (1989) and Klaucke, Hesse, and Ryan (1998) acquired imagery data of the Labrador sea floor including an extensive network of converging drainage channels. Based on seismic and sonar data, distinct differences between submarine and subaerial drainage systems were identified. Mitchell (2004) and Vachtman, Mitchell, and Gawthorpe (2013) described erosion rates and submarine canyon hydrology on the Atlantic continental slope and recommended a simple relationship to describe erosion rates as a function of channel gradient and contributing area. To do so, the authors employed principles of terrestrial hydrology to the submarine environment. An important assumption in developing their model is that long-term erosion rates of branches of fluvial (and thus extended to submarine) channels must be identical. Straub et al. (2007) used high resolution data from the Monterey, CA and Brunei Darussalam continental slopes to assess submarine channel profiles and drainage area statistics. Although substantial differences in physical processes exist, the data yielded submarine scaling exponents within the range of terrestrial observations.

Gamboa, Alves, and Cartwright (2012) provides the most detailed survey of submarine confluences on confined slopes (i.e., submarine canyon confluences). Based on the interpretation and analysis of 3D seismic data, these researchers proposed a classification scheme based on the geometry of the confluence. The classification system is similar to that of river confluences in that they can either be asymmetrical, in

2

which case the downstream reach is in line with one of the contributing channels, or symmetrical, in which case the downstream reach approximately bisects the junction angle between the contributing channels. Confluence densities and width ratios in the study area of Gamboa, Alves, and Cartwright (2012) also indicate similarities to those found in fluvial river systems furthering the notion by Mitchell (2004) and Straub et al. (2007) that submarine channel confluences, from the drainage and hydrological perspective, are similar to those found in terrestrial river systems.

Despite the similarities noted in geometry and erosion rates, hydraulic differences in the confluences of submarine channels inevitably exists due to the nature of density currents. The most significant difference hydraulically is that the density contrast between turbidity currents and the ambient fluid is on the order of only a few percent, whereas fluvial rivers experience a density difference of about 800 times that of the ambient fluid (i.e., air) (Parker, Fukushima, and Pantin 1986; Imran, Parker, and Katopodes 1998). Some aspects of turbidity or density currents have been well documented as analogous to rivers and others have shown distinct differences. Several researchers (e.g., Clark and Pickering 1996; Peakall, McCaffrey, and Kneller 2000; Pirmez and Imran 2003) document the similarities in sinuosity, wavelengths, and avulsions of submarine channels and river channels. Others document the differences in terms of hydraulic and morphodynamic character (e.g., Parker, Fukushima, and Pantin 1986; Wynn, Cronin, and Peakall 2007; Kolla, Posamentier, and Wood 2007; Deptuck et al. 2007; Islam and Imran 2008; Sequeiros et al. 2010; Straub et al. 2011; Ezz and Imran 2014). Parker et al. (1987) noted that since relative density is the driving mechanism of turbidity currents, erosive and flow power are subject to direct feedback from entraining and depositing bed sediment adding complexity to sediment transport potential in submarine flows. Sequeiros et al. (2010) proposed a sediment transport relation which is strikingly similar to that of river systems with reasonable validity. Finally, Straub et al. (2011) showed that levee building in submarine

3

channels can be a result of aggradation rather than incision as is the case with river channels. To the authors' knowledge, no study has been reported regarding hydraulics and sediment response in submarine channel confluences despite the fact that channel networks are important elements of continental margin strata.

This paper presents the results and the analysis of laboratory experiments specifically designed to study simultaneously active, conservative density current confluences over an erodible bed. Using the classification system of Gamboa, Alves, and Cartwright (2012), tests were performed in a neutrally asymmetric confluence (neutrally indicating that both upstream reaches contribute equally to the downstream reach). A total of 21 subsequent density currents were released to characterize the velocity field in the junction and in the contributing channels. In particular, one-dimensional primary (i.e., streamwise) velocity and two-dimensional horizontal velocity in the near junction zone were measured. Further, qualitative assessment of bed evolution was performed after each test. Well-established models for terrestrial river confluences were then tested with the submarine data to identify similarities and differences between subaerial and submarine confluences. This study focused on gaining insight on the hydraulics and mechanics of density current confluences and their morphological impacts, and on observing how the submarine velocity field and erosional patterns compare to their terrestrial river counterparts.

Chapter 2

Background Information on River Confluences

The characteristics and properties of river channel confluences have been examined by field observations (e.g., Best 1988), physical experiments (e.g., Lin and Soong 1979; Best 1988; Gurram, Karki, and Hager 1997; Hsu, Wu, and Lee 1998; Webber and Greated 1966; Qing-Yuan et al. 2009), and theoretical and numerical models (e.g., Lin and Soong 1979; Hsu, Wu, and Lee 1998; Hsu, Lee, and Chang 1998; Shabayek, Steffler, and Hicks 2002; Kesserwani et al. 2008).

Hydraulic characteristics in terrestrial river confluences include a separation zone downstream of the junction, streamline deviation angle from the side channel, and a backwater effect into each contributing reach.

In the confluence of terrestrial rivers, flow separation occurs at the downstream junction point and continues into the downstream reach; the extent of flow separation has been studied by Best and Reid (1984) and Gurram, Karki, and Hager (1997) who both focused on maximum separation zone dimensions, and Qing-Yuan et al. (2009) who studied the variation in separation zone geometry with depth.

Best and Reid (1984) quantified the geometry and extent of the flow separation zone downstream of an experimental, equal-width junction. They varied both relative discharge and junction angle and tracked the extent of the separation zone visually using an overhead camera. The authors found that the length and width of the flow separation zone increase with both relative tributary contribution and junction angle. Best and Reid (1984) fit logarithmic trend lines to their data set for maximum separation zone dimensions as:

5

$$\frac{b_s}{b_3} = 0.264 + 0.117 \ln(\frac{Q_s}{Q_m}) \tag{2.1}$$

$$\frac{L_s}{b_3} = 1.348 + 0.538 \ln(\frac{Q_s}{Q_m}) \tag{2.2}$$

where b_s and L_s are the width and length of the separation zone, respectively, b_3 is the width of the downstream reach, Q_s is the discharge from the side channel, and Q_m is the discharge from the side channel. Gurram, Karki, and Hager (1997) also developed an analytical solution for separation zone geometry in subcritical open-channel flows as:

$$\frac{b_s}{b_3} = \frac{1}{2}(F_{d/s} - \frac{2}{3})^2 + 0.45Q_r^{\frac{1}{2}}(\frac{\theta}{90°}) \tag{2.3}$$

$$\frac{L_s}{b_3} = 3.8 \sin^3 \theta (1 - \frac{1}{2}F_{d/s})Q_r^{\frac{1}{2}} \tag{2.4}$$

where $F_{d/s}$ is the downstream Froude number, Q_r is the discharge ratio, and θ is the junction angle.

Qing-Yuan et al. (2009) furthered the investigation into separation zone geometry by describing the variation of separation zone extent with depth in a 90° open channel junction. In particular, they developed a new method for defining the extent of the separation zone called the velocity isoline method which is based on tracing the zero-downstream-velocity contour to define the separation zone boundary. The careful comparison of the new isoline method with the classical streamline method to determine the extent of the separation zone revealed that the isoline method is simpler to implement if velocity data is available. The main results of the Qing-Yuan et al. (2009) work are, 1) the separation zone at open channel junctions increases both in width and in length away from the bed, and 2) the separation zone becomes more uniform vertically as the side channel contribution decreases.

6

Due to flow separation in the downstream reach of river confluences, effective flow area decreases opposite to the separation zone creating a high velocity region alongside the separation. Best and Reid (1984) defined a velocity index for the maximum near bed velocity as $U_x = U_{\max}/U_1$ where U_x is the velocity index, $U_{\max}$ is the maximum observed velocity in the downstream reach at the separation zone section, and U_1 is the velocity in the main upstream reach. A line was fit to the data as:

$$U_x = 4.52 + 2.36\frac{b_3 - b_s}{b_3} \tag{2.5}$$

Early models of river confluences (e.g., Lin and Soong 1979), termed linear models, assumed equal upstream water depths in each contributing branch. Later models of Hsu, Lee, and Chang (1998) and Gurram, Karki, and Hager (1997), are nonlinear models based on momentum balance in the junction.

Hsu, Lee, and Chang (1998) proposed an analytical approach for solving the upstream depth ratio of subcritical open channel junction flows for equal width, horizontal channels and they found that the upstream depth ratio is directly correlated to the Froude number in the downstream reach, $F_{d/s}$, and to junction angle. The researchers also examined trends of streamline deviation angle across the junction line as a function of discharge ratio and junction angle. The deviation angle is defined as the angle of the streamlines entering the junction from the side channel. The deviation angle is measured relative to the junction line, and the side channel streamlines are skewed from the junction angle due to forcing from the main channel inflow.

The pioneering work of Best (1988), which included both laboratory experiments and field observation, utilized knowledge of junction hydraulics to identify three distinct morphological elements common among open channel junctions: 1) avalanche faces at the upstream edges of the junction zone where the two contributing channels combine, 2) a deep central scour beginning at the upstream junction point and approximately bisecting the junction angle, and 3) the formation of a bar downstream

7

of the separation zone. The dominant factors effecting the geometry of these three elements are relative discharge and junction angle. Best (1988) concluded that increasing either of these factors, i.e., the relative discharge and/or the junction angle, results in a more pronounced segregation of sediment and flow contributions causing 1) the retreat of the main channel avalanche face, 2) rotation of the central scour about the upstream junction point, and 3) increase in the extent of the separation zone bar. Gamboa, Alves, and Cartwright (2012) identified morphological elements of submarine junctions that are similar to those defined by Best (1988), i.e., the presence of plunging faces in the contributing channels and a well defined scour int he junction zone. These observations suggest that by using the well-established knowledge on fluvial channel confluences, analogies between the subaerial and the submarine settings can be established.

By relating protrusion into the junction with relative discharge and junction angle, Best (1988) fit a line to his data for the case of equal contribution from each channel as:

$$\epsilon = 1.9525 - 0.0186\theta \tag{2.6}$$

where ϵ is the normalized distance from the upstream junction point to the farthest point of the avalanche face into the junction and is normalized by the downstream channel width as $\epsilon = a/b_3$ where a is the dimensional maximum extent of the avalanche face into the junction from the upstream junction point.

Best (1988) also developed logarithmic trend lines for the maximum depth of scouring past the avalanche face starting at the upstream junction point. The depth of scouring was normalized by the upstream reaches' water depth and takes the form:

$$d_s = -4.944 + 1.830 \ln \theta \tag{2.7}$$

where d_s is the normalized scour depth defined as $d_s = d/(Y_{avg})$ where d is the

8

dimensional scour depth and Y_{avg} is the average water depth of the main and side channels at the junction entrance.

Best (1988) has described the orientation of the line of maximum scour as approximately bisecting the junction angle which was computed from the curve for equal upstream discharge taking the form:

$$\beta = 6.98 + 0.297\theta \tag{2.8}$$

where β is the angle of the maximum scour line relative to the main channel direction originating from the upstream junction point.

CHAPTER 3

LABORATORY EXPERIMENTS

3.1 EXPERIMENTAL SETUP AND PROCEDURE

The laboratory experiments were conducted in an asymmetric y-shaped flume in the Hydraulics Laboratory at the University of South Carolina (Figure 3.1). Experimental conditions are summarized in Table 3.1.

Experimental Conditions

The rigid sub-bed of the flume was constructed with painted wood. The walls were painted wood on one side of the flume and transparent acrylic glass on the other side for flow visualization and tracking of the density current's propagation.

The near-junction zones, to a distance of 0.91 m in the upstream direction and the entire length of the downstream reach, was covered to a depth of 40 mm with sand-sized plastic particles with a specific gravity of 1.5 and D_{50} of 0.2 mm. The extreme upstream reaches of each inflow channel was a painted wood board to allow the current to develop fully before reaching the erodible bed material. The board was also 40 mm deep to avoid any bed discordance.

A premixed salt water solution was stored in a continuously stirred overflow tank from which it was lifted to a constant-elevation head tank. The head tank split in a manifold to feed each upstream reach. Each limb of the manifold was equipped with differential piezometers and valves to monitor and ensure constant inflow throughout testing. Each branch of the flume was equipped with a momentum-reducing discharge

10

box and grate to ensure the inflow was quiescent and the density current could form in a relatively short downstream distance. The discharge boxes were elevated to 100 mm above the flume bed to allow the inflow mixture to plunge to produce a coherent density current. The flume's downstream reach terminated in a large tank where the density current was allowed to plunge below the flume's bed elevation. The ambient water level was maintained with an overflow drain pipe in the downstream tank.

Test Procedure

In preparation for each test, 1.28 m^3 of a salt water mixture was prepared to a density of 1035 kg/m^3. To this end, a bench test was performed to determine the precise mass of salt required for each incremental change in fluid density. Using the results of the bench test, a formula was developed based on the initial density of the fluid and target density as:

$$\frac{m_{salt}}{\forall} = 1.366 \times (\rho_{target} - \rho_{initial}) \tag{3.1}$$

where m_{salt} is the required mass of salt in kg, $\forall$ is the volume of the container in m^3, ρ_{target} is the desired final density of the solution in kg/m^3, and ρ_{initial} is the initial density of the water in kg/m^3. Since, depending on the run time off each test, the entire pre-mixed volume was not fully used, before the subsequent test the mixing tank was refilled with fresh water, mixed, and the initial density was measured in preparation for the new mixture. This procedure resulted in reliably constant inflow density for all tests.

Before the test runs begin, the flume was filled with fresh water, and a continuously operating submersible pump was used to elevate the salt water mixture to a head tank. Once the head tank begins to overflow back to the storage tank for a suitable amount of time, testing can begin. For the duration of the test, a calibrated discharge pump was operating in the downstream tank to remove the dense water as it plunges out

of the flume. In tandem, a constant, low-velocity inflow of fresh water was added to the top of the downstream discharge tank to reduce upward convection of dense water in the downstream tank and to prevent reflection. Each test was initiated by simultaneously opening valves releasing the salt water mixture to each flume. Using the differential piezometers, all tests showed a constant inflow of 1.78 L/s ($\pm 2\%$) to each channel. The discharge started in the momentum-reducing boxes, passed the flow-straightening grates, and formed two developed density currents. The currents' heads propagated downstream, collided at the junction, and continued downstream. Once the head of the combined current exited the domain and the current height stabilized, measurement procedures began.

Once the pre-mixed volume of salt water was nearly depleted, the test was halted by closing the inflow valves to each discharge box. The current tail was then allowed to move downstream where the discharge pump and drain were still active until the current exited the domain completely. The flume was then drained to approximately one-third of the initial depth, and photographs of the bed were taken. To avoid any bed disturbance, the flume was never completely drained below this point between tests; rather, the flume was slowly refilled with fresh water and drained repeatedly until the water density was measured to be 1000 kg/m^3, as desired, for subsequent testing.

Measurement Techniques

Measurements were taken to capture the current depth in space, 1D velocity profiles, 2D horizontal velocity, and bed evolution after each test. A high-definition camcorder was mounted along the flume's main channel to capture the current development in space and time. In preliminary testing, these cameras were also used to ensure the side and main channels were behaving similarly in terms of density current development and propagation. Ultrasonic velocity profilers (UVPs) were mounted at an angle of

12

45° pointing downward into the current for 1D primary velocity measurement as a function of depth. These probes were placed at the centerline of the main and side channels and downstream reach. UVPs were also used in a grid pattern to obtain 2D horizontal velocity at 114.3, 88.9, 63.5, 38.1, and 25.4 mm from the bed. The near-bed 2D velocity was used to correlate to observations on bed development. A still overhead camera was used to photograph the bed of the main channel after each run. For better quality of the photos, several photos were taken at a short distance from the bed and merged to one image. The photos were overlapped approximately 30% on each side to avoid distortion in the final image.

3.2 FLOW FIELD

Given equal inflow discharges to each flume, behavior of each upstream reach was established to be equal by obtaining primary, or downstream, velocity profiles in the channel centerlines at 1.092 m from each discharge boxes. Figure 3.2 shows the normalized velocity profile from each channel and good agreement is observable. The peak velocity is within 8% in each channel with similar shape and inflection (near $z/H = 1$). In the figure, z is the upward coordinate from the bed, u is the measured primary velocity, and U and H are the depth averaged velocity and current height, respectively, by using the moment method (Parker et al. 1987). Since matching between the side and main channel is good, henceforth measurements and discussion will focus on the main upstream channel, junction zone, and the downstream reach.

In the laboratory tests it was observed that the current rose into the ambient water layer in the junction as seen in Figure 3.3 taken during the initial collision of the current fronts. After the two inflows combined, they re-plunged in the downstream reach. This large plume subsided to a quasi-equilibrium height which is represented in the velocity profiles of Figure 3.4 and the depth-averaged H in Figure 3.5. The implications of the rising-plunging in the quasi-steady condition is later discussed.

13

Primary Velocity

Figure 3.4 shows one-dimensional primary velocity along the main channel centerline. The dashed vertical lines in the figure indicate the upstream and downstream junction points, and the solid vertical lines indicate the measurement point downstream coordinate. The maximum velocity near the junction shifted away from the bed near the downstream junction point and then returned to a more typical velocity profile in the downstream reach.

Figure 3.5 shows the layer-averaged current thickness, H, and velocity, U based on the profiles seen in Figure 3.4. As expected for the majority of the domain, H and U were inversely correlated, but both increased near the downstream junction point. This suggests that in the junction zone, there was significant upward convection of momentum causing the maximum velocity to be further from the bed and flow area to increase.

Horizontal Velocity

Two-dimensional horizontal velocity measurements were taken near the junction at five different elevations above the bed. Isovelocity maps are shown in Figure 3.6; the entire width of the main channel is not included in these measurements due to the need for physical clearance of the velocity probes. In general, velocity in the junction zone and downstream of the junction was higher closer to the bed as expected based on the one-dimensional velocity profiles in Figure 3.4. At all of the five elevations near the upstream junction point, horizontal velocity was low with acceleration through the junction zone and in particular downstream of the junction. Some flow separation can be noted just beyond the downstream junction point which is more evident away from the bed.

Horizontal velocity vectors with streamlines are shown in Figure 3.7. A clear shear plane between main- and side-channel contributions can be seen in this figure.

14

Near the bed, the main channel contribution was restricted to the outer wall of the downstream reach as the side channel inflow entered the junction. Conversely, the main channel contribution was more dominant away from the bed. This implies that the main channel flow rode atop the side channel flow in the junction before mixing in the downstream reach where velocity was once again unidirectional. The stagnation of flow near the upstream junction point seen in the horizontal velocity contour plots (Figure 3.6) can also be seen in the streamlines plots (Figure 3.7) where streamlines near the upstream junction point in the main channel terminate against the shear plane of contributing inflows. Flow separation in the downstream reach is also evident in termination of streamlines against the wall of the flume at elevations far from the bed. It can be inferred that the main channel inflow rode atop the side channel inflow and entrained ambient water, thus becoming more diffuse and weaker. Its ability to counteract the momentum from the side channel lessened allowing for the formation of a downstream separation zone. Near the bed, the orientation of the downstream reach and strength of the main channel inflow forced the side channel contribution to deviate to the downstream direction and stick to the wall of the flume.

3.3 BED EVOLUTION

Figure 3.8 shows the evolution of the erosional pattern observed on the bed. The inflow condition was such that sufficient shear stress was acting on the bed to create distinctive bedforms upstream and downstream of the junction zone, but very little sediment transport was noted in the junction zone itself. This corroborates the notion that horizontal momentum was converted to vertical momentum in the confluence zone as the main channel inflow rose above the side channel inflow. Thus horizontal shear stresses acting on the bed were reduced inhibiting transport of bed material.

The most distinctive bathymetric pattern was the scouring beginning at the downstream junction point and continuing across the width of the downstream reach of

15

Table 3.1   Experimental conditions.

Inflow density	1035 kg/m^3
Ambient density	997 - 1000 kg/m^3
Discharge per channel	1.78 L/s
Discharge area	304.8 mm X 50.8 mm (W X H)
Elevation of discharge box	100 mm
Constant ambient water depth	457 mm
Junction angle	45°
Run time per test	450 - 570 s

the flume. The avalanche face (i.e., beginning of the scoured section) was approximately in line with the side channel's wall and developed a series of relatively deep erosional waves from successive runs until reaching the opposite wall (Figure 3.9). By comparing the scouring to the near-bed velocity contours (Figure 3.6), it is clear that this zone downstream of the junction experiences the highest horizontal velocity, thus scouring here is expected.

Figure 3.10 shows the near-bed velocity and associated scouring downstream of the junction. From this plot it is clear that in the junction there was relatively low horizontal velocity thus sediment transport capacity was limited. However, downstream of the junction, high horizontal velocity indicates high bed shear stress which surpasses the critical threshold of motion for this sediment.
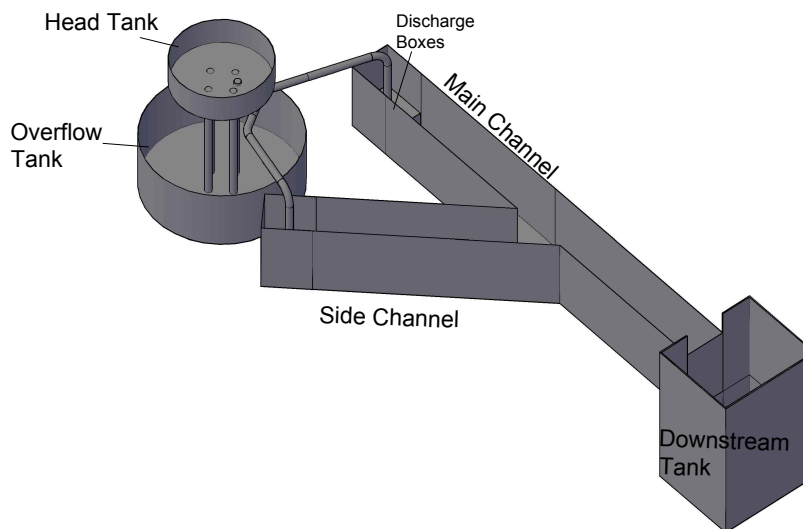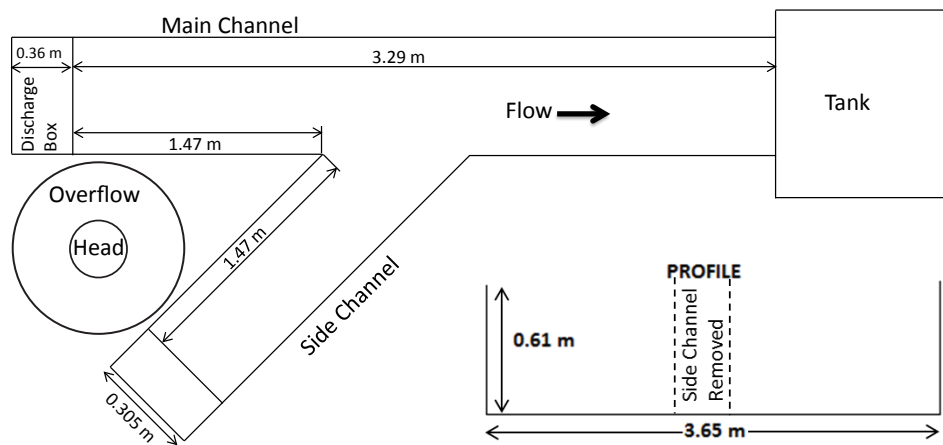
16

Figure 3.1   Physical model dimensions in plan view, profile view, and rendering.
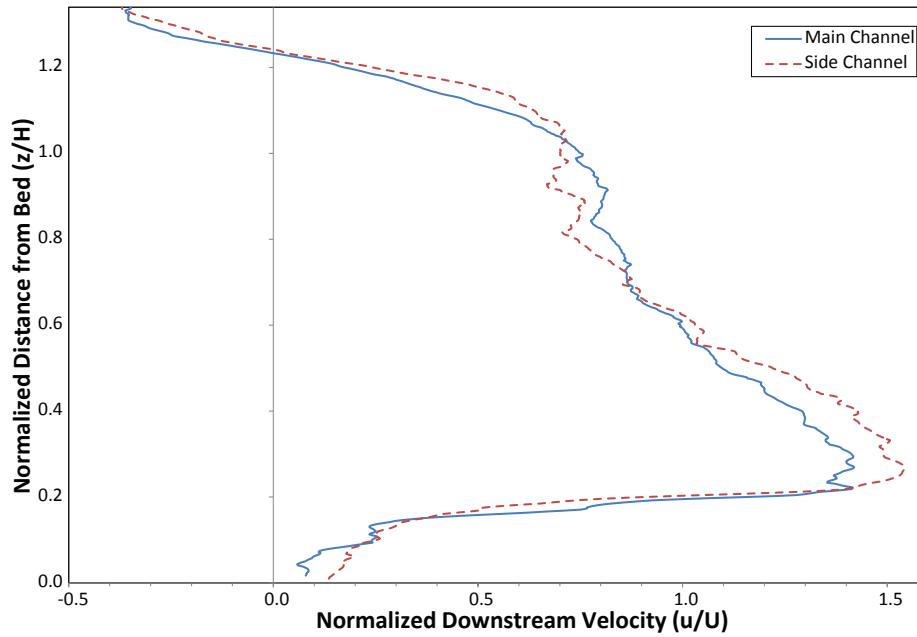
Figure 3.2   Comparison of main channel and side channel primary velocity at the channel centerlines.
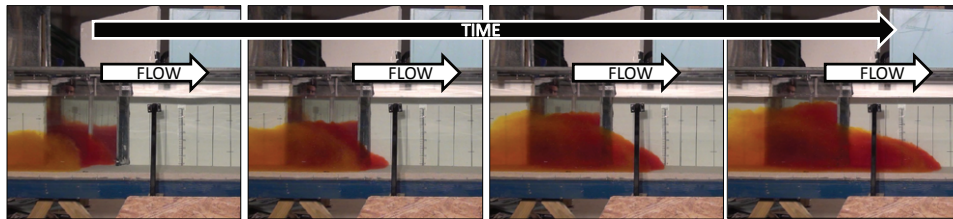

Figure 3.3   Initial head confluence of the density currents in time as seen from the main channel.
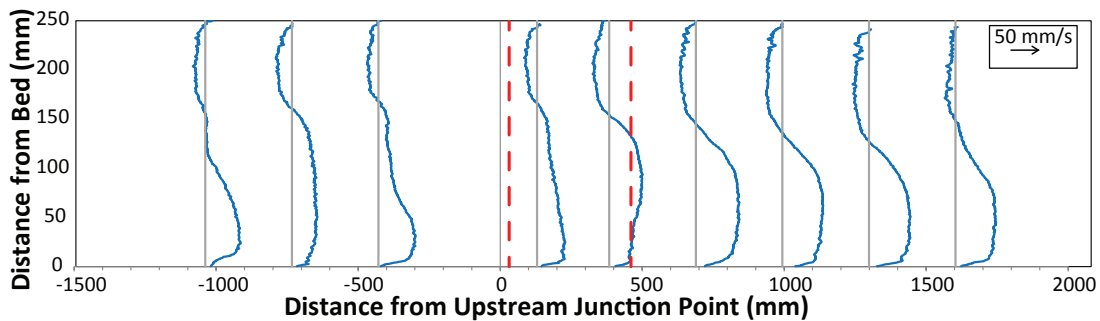
Figure 3.4   Primary velocity profiles along the main channel centerline. Solid vertical lines indicate the points of measurement, and dashed vertical lines indicate the location at which the side channel connects.
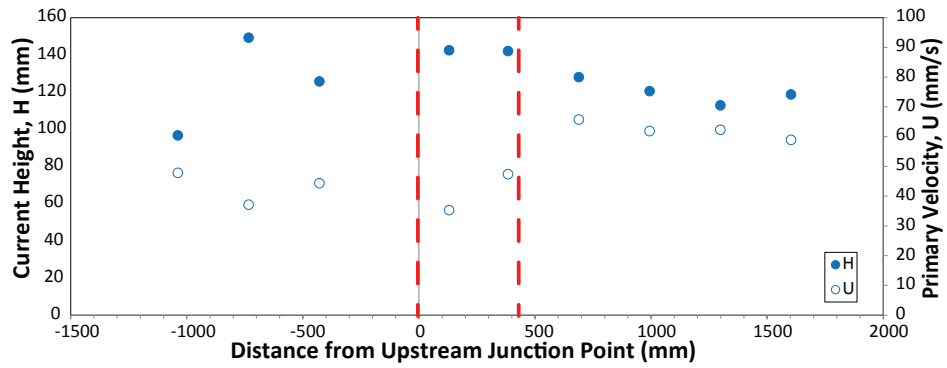
Figure 3.5   Layer averaged current height and velocity based on 1D profiles.

19
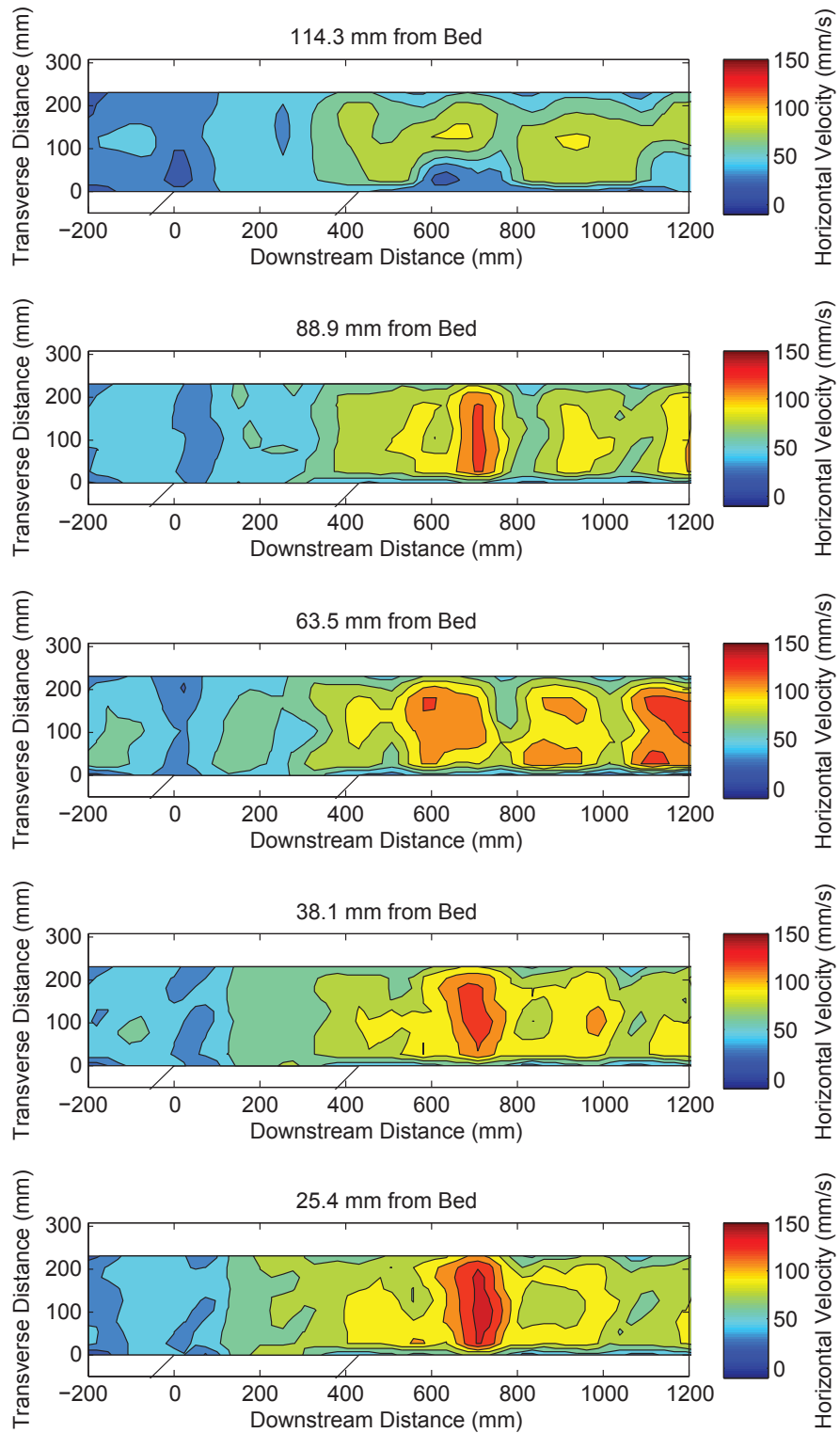
Figure 3.6 Horizontal isovelocity map near the junction zone at 114.3 mm, 88.9 mm, 63.5 mm, 38.1 mm, and 25.4 mm from the bed. The origin of the plot is the upstream junction point.

20
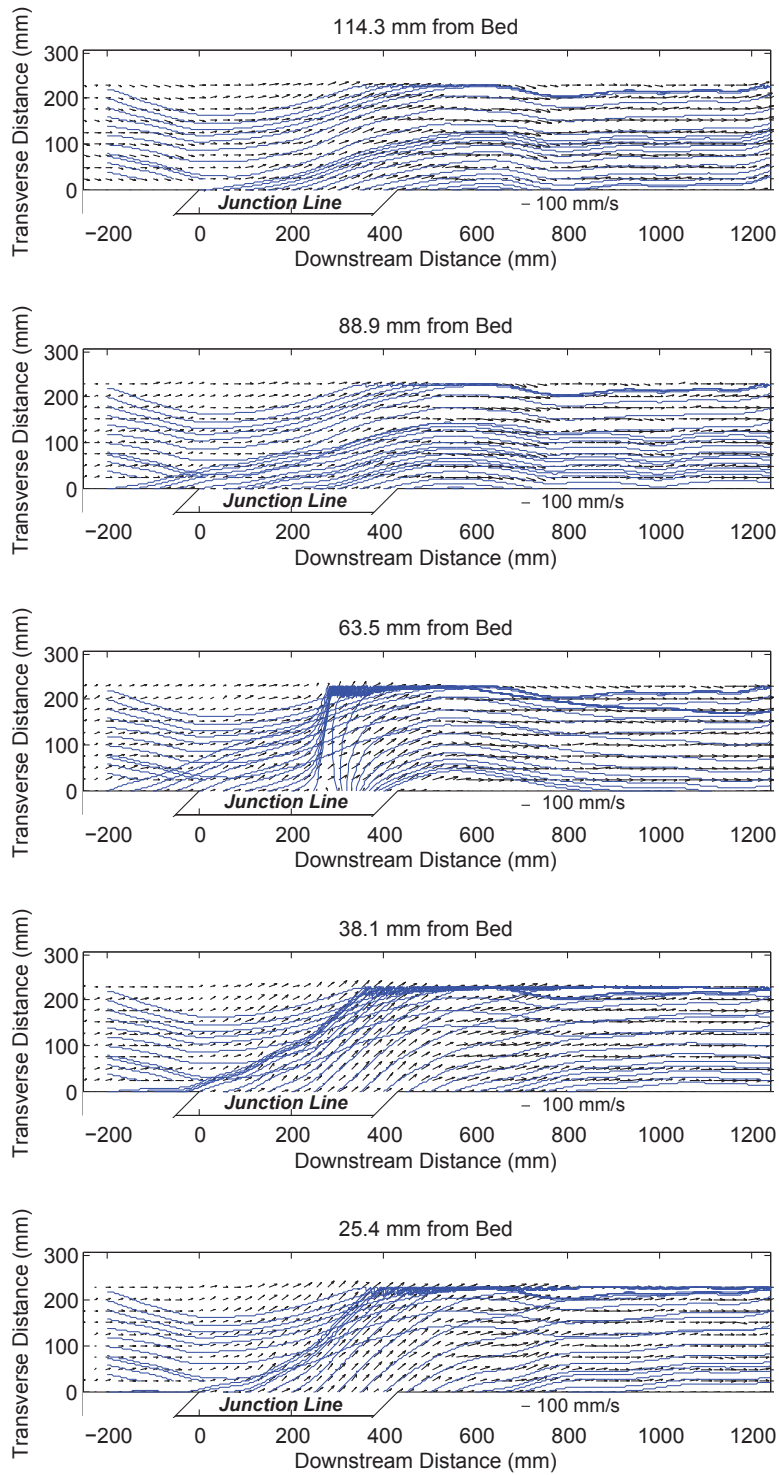
Figure 3.7   Horizontal velocity vectors with streamlines near the junction zone at 114.3 mm, 88.9 mm, 63.5 mm, 38.1 mm, and 25.4 mm from the bed. The origin of the plot is the upstream junction point.
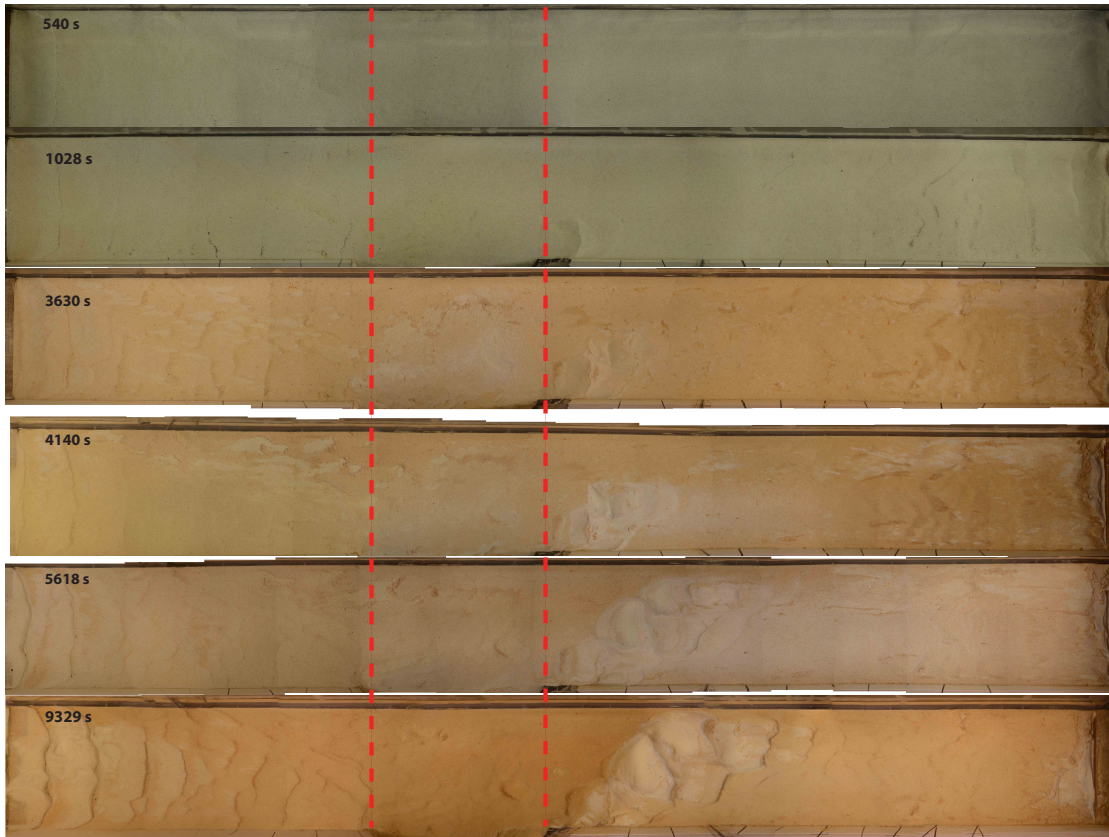
Figure 3.8   Evolution of the bed of main channel after 540 s, 1028 s, 3630 s, 4140 s, 5618 s, and 9329 s total run time. Flow is from left to right, and the vertical dash lines indicate the locations of the junction points.
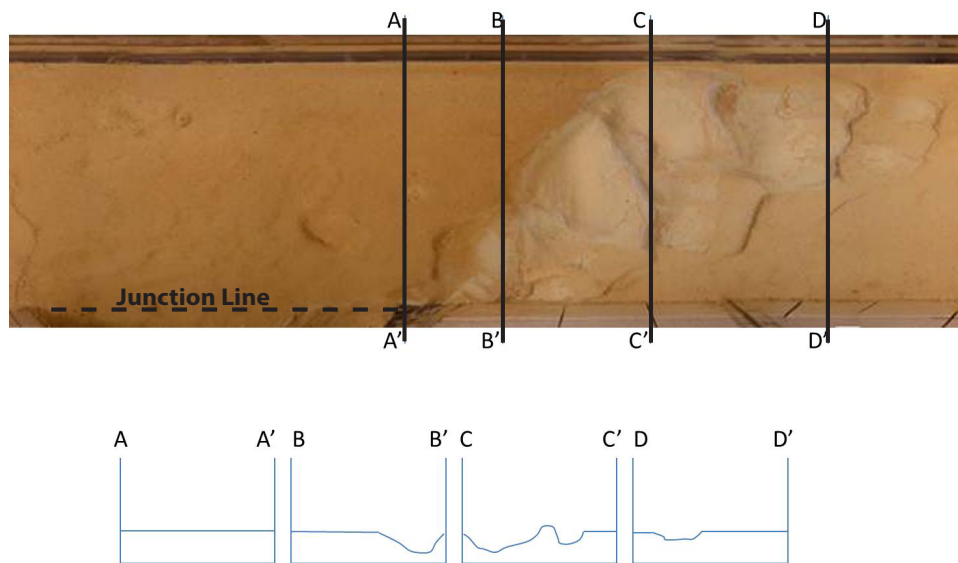
Figure 3.9   Qualitatively observed erosional pattern downstream of the junction.
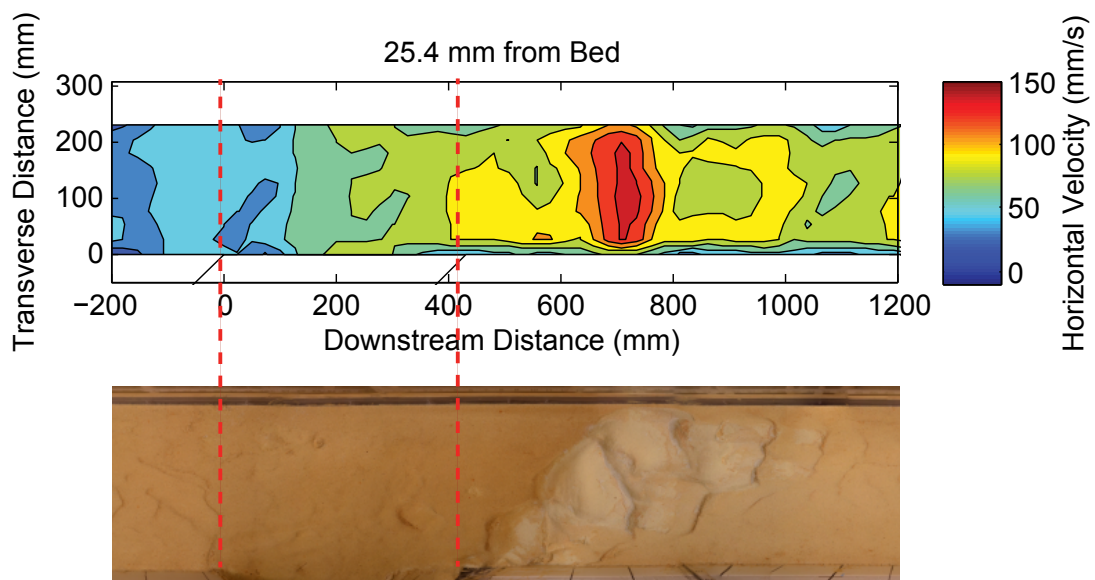
Figure 3.10   Near-bed velocity isoline plot with associated scouring downstream of the junction. The dashed vertical lines indicate the endpoints of the junction line.

23

Chapter 4

Comparison to River Confluences

4.1 Comparison to River Hydraulics

With the previously discussed observations and measurements, comparisons can be directly made to well-established observations of subaerial river confluences. This comparison will focus on comparing hydraulic response to the confluence as described by Best and Reid (1984), Gurram, Karki, and Hager (1997), Hsu, Lee, and Chang (1998), and Qing-Yuan et al. (2009). Morphological characteristics of river confluences are extracted from the work of Best (1988). Hydraulic characteristics to be assessed include 1) flow separation downstream of the junction; 2) maximum velocity due to the effective flow contraction adjacent to the separation zone; 3) deviation angle of streamlines entering from the side channel; and 4) backwater effect of the junction into the upstream reaches. Morphological features that are assessed include 1) avalanche faces at the edge of scouring in the junction zone; 2) maximum scouring depth; and 3) maximum scouring orientation. Figure 4.1 shows these characteristics as expected in river confluences with a summary of the characteristics found in the density current case.

Separation Zone

The zero-velocity contour at most elevations are hardly visible in the contour plots of Figure 3.6. Furthermore a closer view and finer contouring revealed only minimal extent of zero primary velocity in the channel near the downstream junction point.

24

Figure 4.2 shows closer views of the streamlines presented in Figure 3.7. Very distinct separation can be seen for the upper three elevations at which horizontal velocities were measured. It is also clear from this figure that near the bed, flow does not separate from the downstream wall. To define coordinates of the streamline delineating the separation zone, the farthest streamline downstream to reattach to the wall was traced upstream to its point of origin. This data is summarized in Table 4.1 in which $x1$ and $x2$ are the downstream coordinates of the streamline beginning and end, respectively, and L_s and b_s are the separation zone length and width, respectively. By comparing the ability to define the separation zone by either the streamline or isoline method, it was found that the streamline method performs better than the isoline method when velocity data is available.

By applying Equations 2.1-2.4 to the current work, the predicted maximum width and length of the separation zone are presented in Table 4.1. In both models, separation zone width is over predicted and length is under predicted. The model of Best and Reid (1984) matched modestly better than the analytical solution of Gurram, Karki, and Hager (1997) indicating that although separation can occur in the case of density currents, application of an analytical solution solved for subaerial flows is inappropriate for application for submarine flows.

To apply the Gurram, Karki, and Hager (1997) solution, $F_{d/s}$ was computed as:

$$F_{d/s} = \frac{Q_t}{(g'b_3^2 H_3^3)^{\frac{1}{2}}} \tag{4.1}$$

where Q_t is the total discharge, and H_3 is the height of the density-ambient fluid downstream of the junction, thus $F_{d/s} = 0.428$ for the present work.

Best and Reid (1984) also discussed separation zone shape index defined as b_s/L_s which linearly trends with discharge ratio. The shape index in the present work is 0.07 which is far from the expected value of 0.19 using the Best and Reid (1984) model. It was observed that separation only occurred in the low-density part of the

25

water column where the main channel contribution rode atop the side channel inflow. If discharge ratio decreases less rising is expected in the junction. This would lead to lesser upward diffusion in the junction zone and a smaller separation zone. The result would be that the size of the separation zone, like in river cases, directly correlates to discharge ratio.

With limited data points, similar assessment to that of Qing-Yuan et al. (2009) on the present work was made with results shown in Table 4.1. As in the work of Qing-Yuan et al. (2009), separation zone length and width increased away from the bed, and it is expected that the maximum separation zone dimensions occurred between $z = 88.9$ and 63.5 mm., very near the depth averaged current height downstream of the junction. Flow separation did not exist in the lower part of the current where concentration and velocity were relatively high. In the upper more diffuse part of the current, flow separation with depth trends similar to river confluences, although with significantly smaller dimensions. As is the case with rivers, the largest flow separation occurred away from frictional boundaries, which includes both the channel bed and dense-ambient interface for density currents.

Maximum Velocity

By applying Equation 2.5 to the data of the present work, predicted velocity index is 2.59, and predicted $U_{\max} = 152.6$ mm/s. The observed maximum velocity from measurement was found to be 157.1 mm/s, less than 3% relative error. To apply this model, the layer averaged velocity in the main channel upstream of the junction was used. This close match indicates that based on upstream velocity, relative discharge, and junction angle, maximum velocity is predictable. However, in the case of rivers, maximum velocity at this location occurs due to constriction of the effective area by the presence of a flow separation zone. In the case of a density current, maximum primary velocity did occur adjacent to the separation zone, but no separation zone

26

was observed near the bed where the maximum velocity occurs. It is postulated that the high velocity measured near the bed in the physical experiments herein were due to convection of vertical to horizontal momentum just downstream of the junction. As discussed previously, in the junction zone, the main channel contribution rode atop the side channel contribution converting horizontal momentum to vertical momentum. After the confluence, dense fluid returned to its layer of natural buoyancy by plunging towards the bed. To confirm this notion, vertical velocity data should be obtained and analyzed for trends downstream of the junction zone.

Deviation Angle

Figure 4.3 shows the variation of deviation angle from the upstream to downstream junction points normalized by the length of the junction line. The values presented are averaged in depth over the five elevations measured as analyzed by Hsu, Lee, and Chang (1998). In general, this is unlike the trend seen by Hsu, Lee, and Chang (1998) who observed that deviation angle decreases for 90% of the distance from upstream to downstream junction points before again increasing near the downstream junction point. The cross-sectionally averaged deviation angle was computed as 35.5° which also is far from the expected 24.5° as predicted by Hsu, Lee, and Chang (1998).

There is a clear trend in the variation of deviation angle with depth in the case presented herein. Figure 4.4 shows average deviation angle with depth normalized by the elevation of the dense-ambient interface upstream of the junction. The dense-ambient interface was determined visually by dying the inflow and measuring the elevation of the dye near the junction (Figure 4.5). The trend shows that the deviation angle near the bed will tend to the junction angle and will approach zero near the elevation of the dense-ambient interface upstream of the junction. The fitted equation takes the form:

27

$$\delta = -\theta\hat{z}^2 + \hat{z} + \theta \tag{4.2}$$

where $\hat{z}$ is the elevation from the bed normalized by dense-ambient interface elevation, and δ is the deviation angle relative to the downstream direction.

Backwater Effect

Two approaches were taken in this work to measure upstream and downstream depths of density current flow. These included layer averaged current height as computed using the moment method, and the other was done visually through photographic capture of the current in the vicinity of the junction (Figure 4.5). Table 4.2 shows the measured values of density current height upstream of the junction and the predicted values by using the Gurram, Karki, and Hager (1997) and Hsu, Lee, and Chang (1998) models. Note that both models perform well for either method of measurement. However, the visual method outperforms the moment method by resulting in less than 1% error for both models and does not require velocity profile measurement. The advantage of the Hsu, Lee, and Chang (1998) model is the independence of streamline deviation angle but only offers a family of curves for predicting backwater effects. Gurram, Karki, and Hager (1997) however, offers a closed form equation for computing backwater depths but requires trial and error or other convergence methods.

4.2 Comparison to River Morphodynamics

The work of Best (1988) is used to evaluate the morphological character of river junctions. The characteristics of avalanche faces, scouring depth, and scouring orientation are assessed and compared to what has been observed in the density current case tested in the present work.

28

Avalanche Faces

As observed in the bed evolution photos, there was no scouring near the upstream junction point, thus no avalanche faces as defined by Best (1988). However, if the avalanche face is defined as the edge of scouring from the downstream junction point, where scouring begins in the density current case, the extent of the avalanche face into the downstream reach can be measured. Figure 4.6 shows how the location of the avalanche face was measured to 307 mm. Note that the avalanche face was oriented at approximately the same angle as the junction angle. By applying Equation 2.6 for the density current case, $\epsilon = 1.12$, and the predicted avalanche face protrusion is $a = 341$ mm. This shows that, with only 11% relative error from the observed to predicted protrusion length, avalanche faces in density currents behave similarly to that seen in rivers but with the origin of scouring being shifted from the upstream junction point in the case of rivers to the downstream junction point in the case of density currents.

Maximum Scour Depth

By applying Equation 2.7 to the conditions in the current work, $d_s = 2.02$ and $d = 267$ mm. To compute d_s, Y_{avg} was taken to be the depth using the visual method discussed previously. The observed scouring depth had an approximate maximum of only 30 mm.

It is clear that the scouring in the density current case is significantly smaller than that observed in river cases. The model of Best (1988) does not directly account for physical parameters such as sediment characteristics and near-bed velocity. In the case presented herein, synthetic particles were used with low specific gravity and grin sizes in the fine sand range which cannot be accounted for in the Best (1988) model. High shear stress acting on the bed is the mechanism that causes scouring and is directly correlated to near-bed velocity which also does not appear in the Best (1988)

model. Best (1988) indirectly accounts for relative velocity in the junction zone and upstream channels through the upstream depth of water. For river junctions, relatively high acceleration is expected as twice the discharge, for $Q_r = 0.5$, passes through a smaller combined channel section. In the case of density currents, twice the discharge passes the junction but is easily diffused to the ambient layer due to very low effective gravity, effectively increasing the flow area of dense fluid. Thus, the relative velocity in the junction zone and upstream channels behave differently in the submarine and subareal cases.

Maximum Scour Orientation

Figure 4.7 shows the orientation of the line of maximum scour for the density current case as 25° and the predicted value using Best's model (Equation 2.8) as 20°. Note again that the origin of the line of maximum scour in the present case is the downstream junction point rather than the upstream junction point.

In the density current case presented herein, β is slightly larger than one-half of the junction angle, and the predicted orientation of maximum scour is slightly smaller than one-half of the junction angle. This is an indication that the simple linear model presented by Best (1988) fits reasonably well with the density current case for maximum scour orientation. Coupled with the good performance of the Best (1988) model for avalanche face (i.e., beginning of scouring) protrusion downstream, the geometry of the scouring can be well predicted by Best (1988) although depths of scouring differ by nearly one order of magnitude.
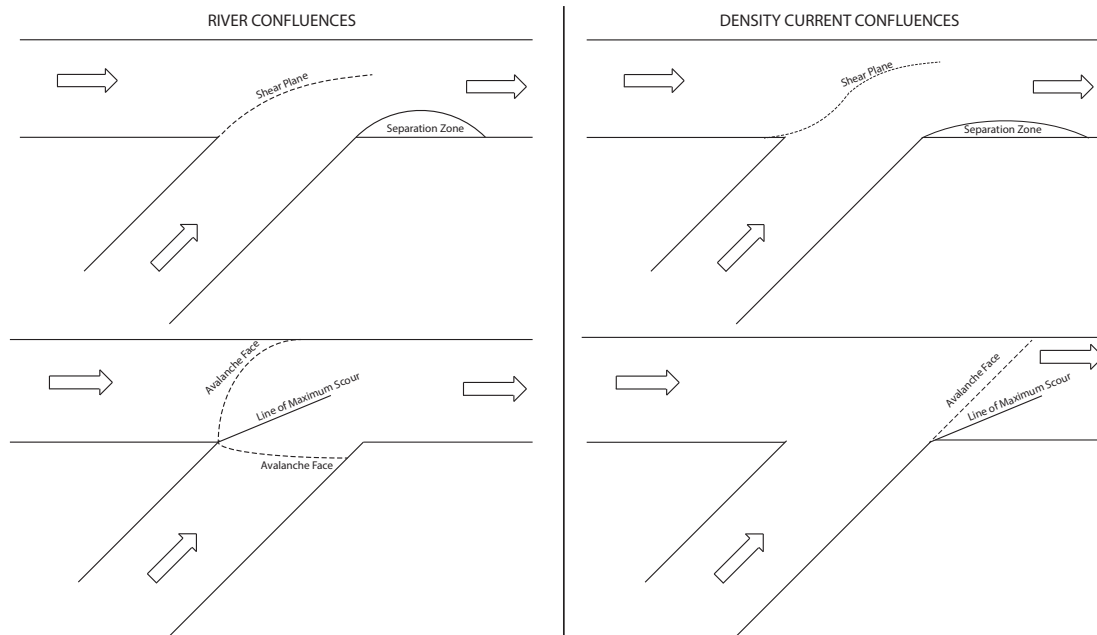
30

Figure 4.1   Typical characteristics of river channel confluences (left panel) and observed characteristics of density current confluences (right panel).

Table 4.1   Length and width of separation zone by elevation and predicted maximum dimensions.

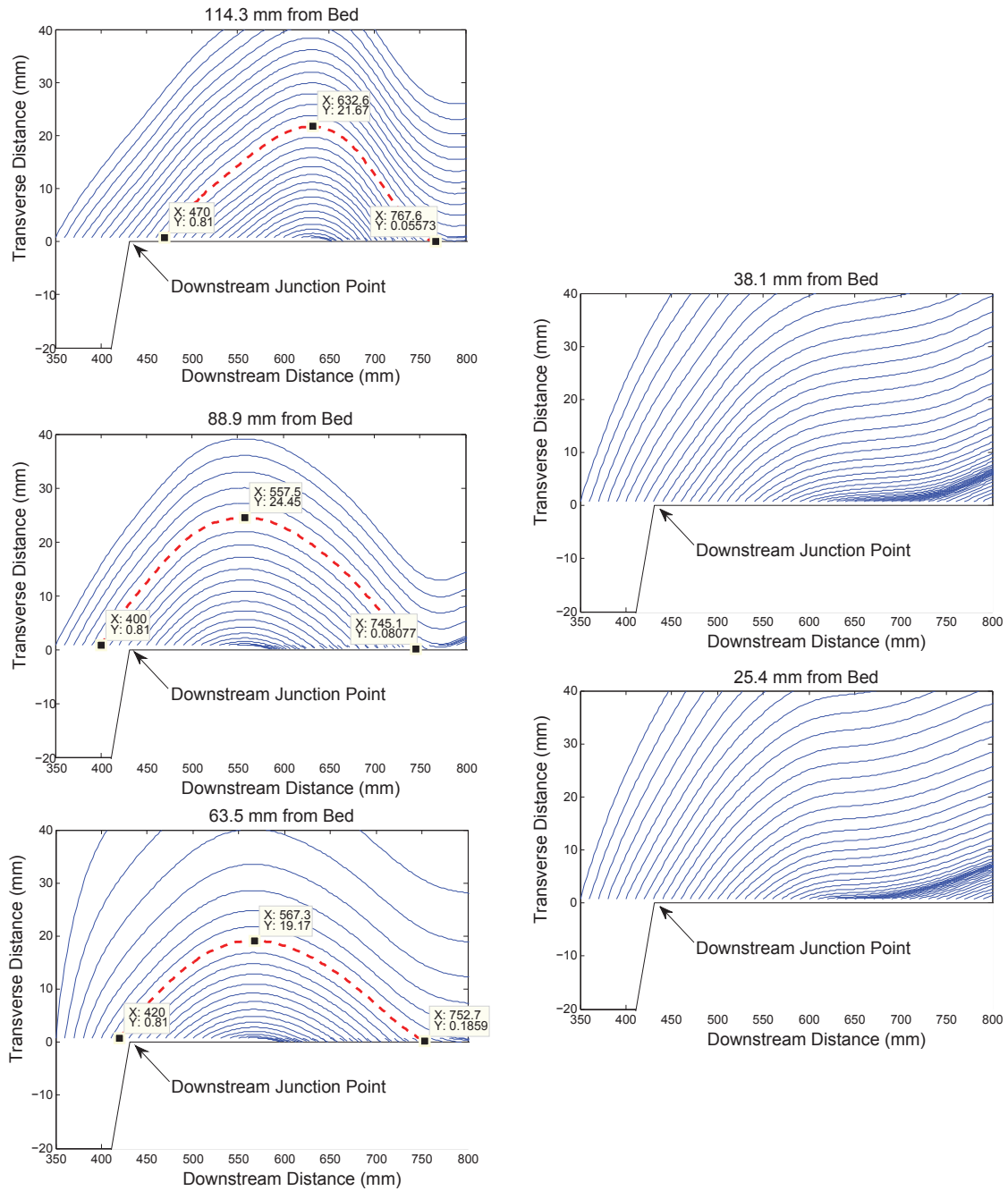| Elevation (mm)	x1 (mm)	x2 (mm)	L_s (mm)	b_s (mm)
114.3	470	767.6	297.6	21.67
88.9	400	745.1	345.1	24.45
63.5	420	752.7	332.7	19.17
38.1	-	-	-	-
25.4	-	-	-	-
Best & Reid	-	-	297.2	55.8
Gurram et al.	-	-	227.6	57.2

31

Figure 4.2   Zoomed streamlines near flow separation zone. The dash line indicates the extent of the flow separation zone, and the coordinates X and Y indicate the downstream and lateral coordinates, respectively, of the points of interest.
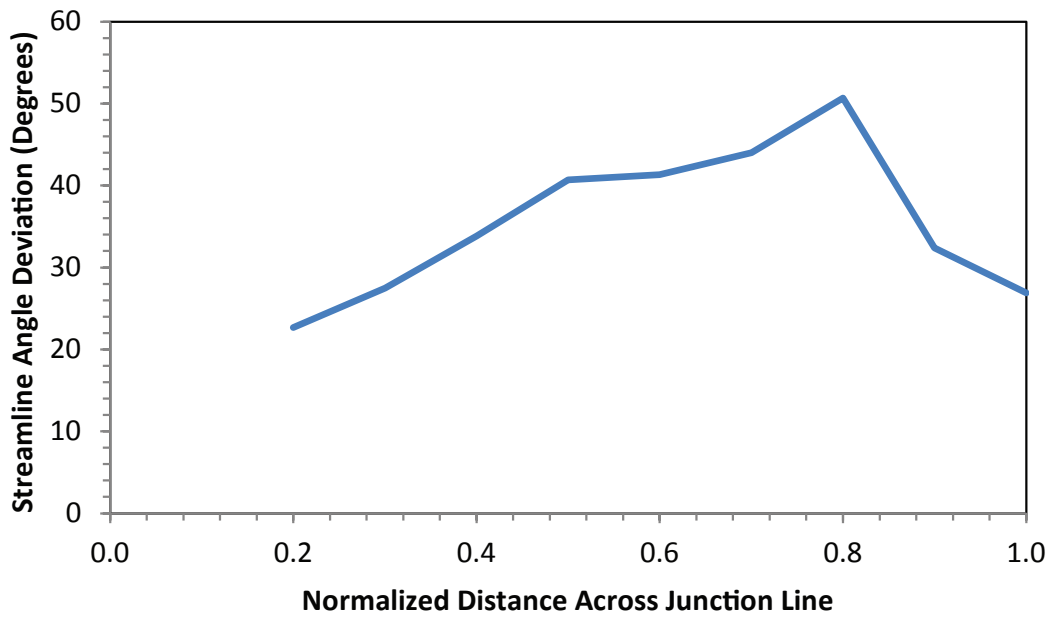
32

Figure 4.3   Variation of streamline deviation angle from the upstream to downstream junction points.
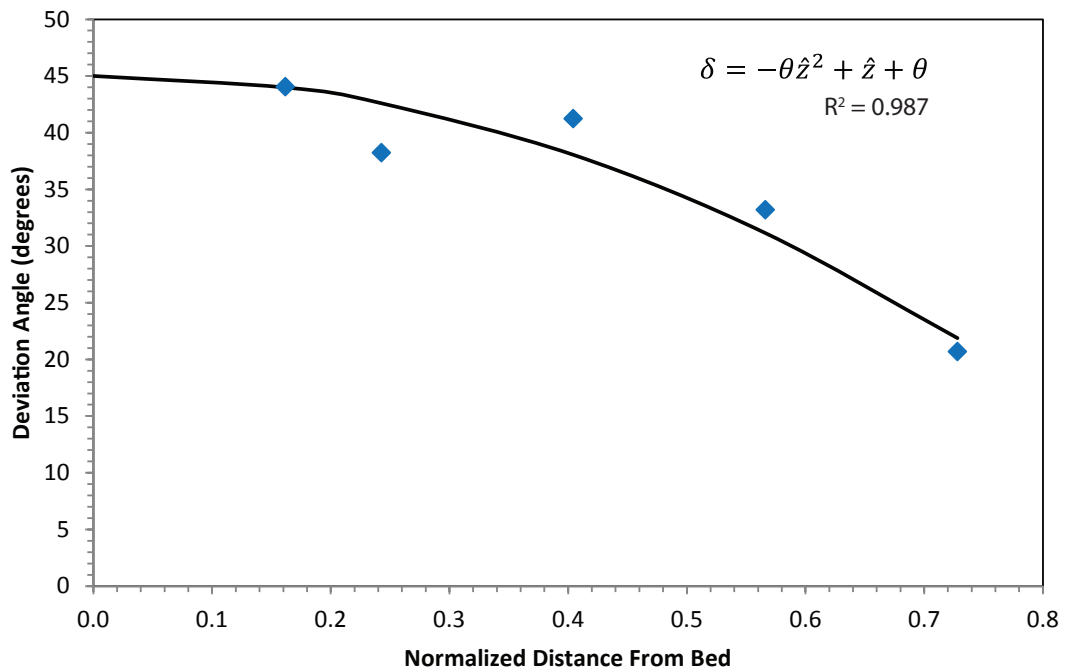

Figure 4.4   Variation of streamline deviation angle with depth. Included is the fit curve to the density current case.
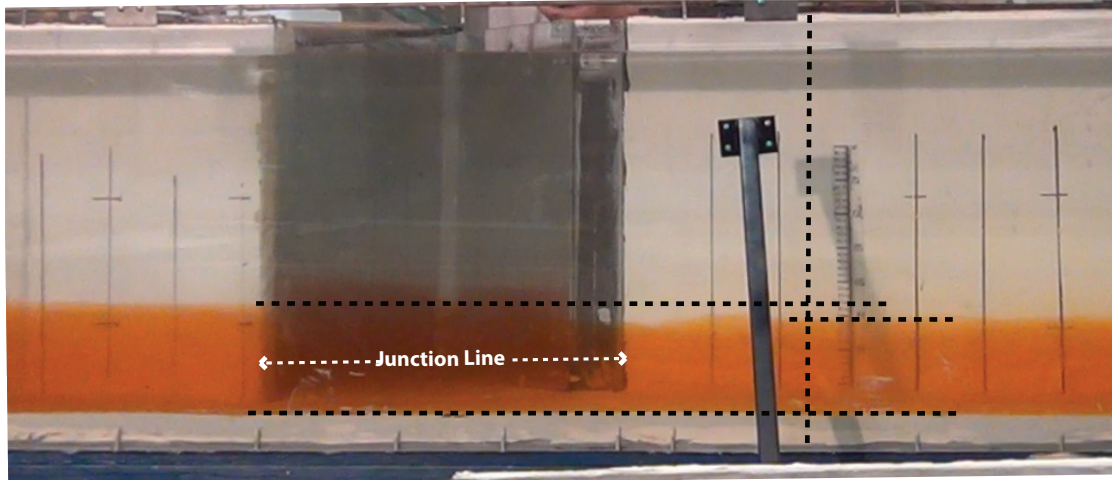
Figure 4.5   Visual method for measuring current height downstream and upstream of the junction.

Table 4.2   Measured and predicted upstream depth due to backwater effect. Each method of current height measurement was separately analyzed, and the measured downstream depths were used to compute the predicted upstream depths. All dimensions are in mm,

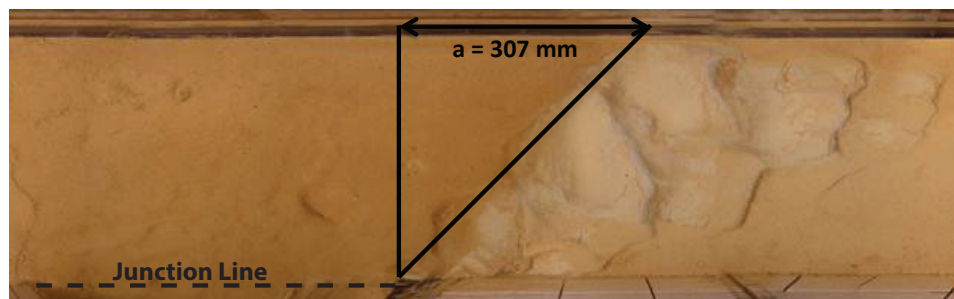|	Moment Method Height	
	Downstream	Upstream
Measured	128.0	142.5
Gurram	128.0	151.0
Hsu	128.0	151.7
	Visual Method Height	
	Downstream	Upstream
Measured	132	157
Gurram	132	155.8
Hsu	132	156.4

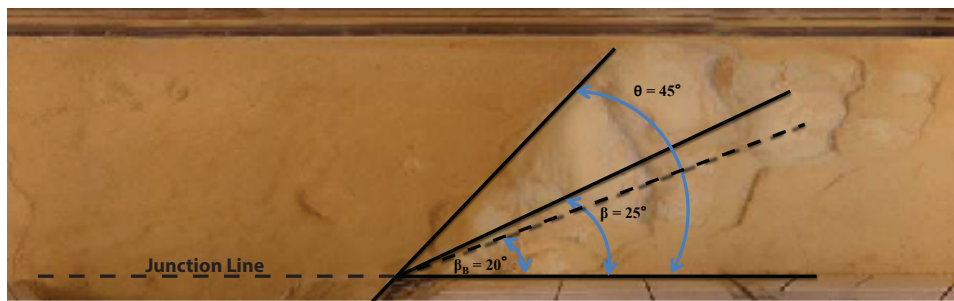Figure 4.6   Location and extent of avalanche face protrusion into the downstream reach.

Figure 4.7   Measured (solid) and predicted (dashed) line of maximum scour.

35

CHAPTER 5

CONCLUSIONS

The presented work includes results from physical experiments on the confluence of two sustained density currents. Also assessed is the applicability of models proposed for subaerial river confluences in terms of hydraulic and morphological characteristics. This work offers a first look at the dynamics and bathymetric implications of such flows. Major observations from the experiments include:

1. Primary velocity showed upward convection in the junction zone.

2. Upward convection of momentum in the junction resulted in reduction of transport capacity at this location.

3. Moving away from the bed, the shear plane between contributing flows rotated towards the main channel direction.

4. Flow separation near the downstream junction point was only observed in the upper, diffuse part of the flow.

5. Maximum horizontal velocity coincided with deep scouring beginning at the downstream junction point.

6. Maximum velocity was caused by re-plunging of the main channel inflow.

7. The streamline method for defining flow separation performed better than the the velocity isoline method.

Assessment of characteristics of the case tested herein revealed similarities to terrestrial river junctions in terms of predicting maximum velocity, backwater effect, avalanche face protrusion, and maximum scour orientation. However, poor correlation between density current and river confluences exists in terms of separation zone dimensions, streamline deviation angle, and maximum scour depths. Notable details of this assessment include:

1. The models of Best and Reid (1984) and Gurram, Karki, and Hager (1997) both over predict separation zone width and under predict separation zone length.

2. Away from frictional boundaries, the separation zone is largest, similar to river confluences.

3. Maximum velocity adjacent to the separation zone is predictable by the model of Best and Reid (1984) but the mechanism of acceleration is conversion of vertical to horizontal momentum rather than flow constriction.

4. Streamline deviation angle across the junction line does not behave similar to river confluences.

5. A simple polynomial function is presented describing the variation of deviation angle with depth based only on junction angle.

6. The backwater effect of density current confluences is predictable by both Gurram, Karki, and Hager (1997) and Hsu, Lee, and Chang (1998) analytical solutions.

7. The visual method for determining current thickness performed better than the moment method for ease of application and good matching with river backwater models.

www.manaraa.com

8. Avalanche face protrusion in rivers and density currents match well with the important distinction that the protrusion in the present case begins at the downstream junction point.

9. Maximum depth of scouring is an order of magnitude smaller in the present case versus that predicted by Best (1988).

10. The orientation of the maximum scour approximately bisects the junction angle for both density current and river cases.

Bibliography

Benjamin, T. B. (1968). "Gravity currents and related phenomena". In: *Journal of Fluid Mechanics* 31.02, p. 209. ISSN: 1469-7645. DOI: 10.1017/s0022112068000133. URL: http://dx.doi.org/10.1017/S0022112068000133.

Best, J. L. (1988). "Sediment transport and bed morphology at river channel confluences". In: *Sedimentology* 35.3, pp. 481–498. ISSN: 1365-3091. DOI: 10.1111/j.1365-3091.1988.tb00999.x. URL: http://dx.doi.org/10.1111/j.1365-3091.1988.tb00999.x.

Best, J. L. and I. Reid (1984). "Separation Zone at Open Channel Junctions". In: *J. Hydraul. Eng.* 110.11, pp. 1588–1594. ISSN: 1943-7900. DOI: 10.1061/(asce)0733-9429(1984)110:11(1588). URL: http://dx.doi.org/10.1061/(ASCE)0733-9429(1984)110:11(1588).

Canals, M., R. Urgeles, and A. M. Calafat (2000). "Deep sea-floor evidence of past ice streams off the Antarctic Peninsula". In: *Geology* 28.1, p. 31. ISSN: 0091-7613. DOI: 10.1130/0091-7613(2000)028<0031:dseopi>2.0.co;2. URL: http://dx.doi.org/10.1130/0091-7613(2000)028<0031:DSEOPI>2.0.CO;2.

Clark, J. and K. Pickering (1996). "Architectural elements and growth patterns of submarine channels: applications to hydrocarbon exploration". In: *AAPG Bulletin* 80, pp. 194–221.

Dalla Valle, G. and F. Gamberi (2011). "Slope channel formation, evolution and backfilling in a wide shelf, passive continental margin (Northeastern Sardinia slope, Central Tyrrhenian Sea)". In: *Marine Geology* 286.1-4, pp. 95–105. ISSN: 0025-3227. DOI: 10.1016/j.margeo.2011.06.005. URL: http://dx.doi.org/10.1016/j.margeo.2011.06.005.

Deptuck, M. E. et al. (2007). "Migration-aggradation history and 3-D seismic geomorphology of submarine channels in the Pleistocene Benin-major Canyon, western Niger Delta slope". In: *Marine and Petroleum Geology* 24.6-9, pp. 406–433. ISSN: 0264-8172. DOI: 10.1016/j.marpetgeo.2007.01.005. URL: http://dx.doi.org/10.1016/j.marpetgeo.2007.01.005.

39

Ezz, H., A. Cantelli, and J. Imran (2013). "Experimental modeling of depositional turbidity currents in a sinuous submarine channel". In: *Sedimentary Geology* 290, pp. 175–187. ISSN: 0037-0738. DOI: 10.1016/j.sedgeo.2013.03.017. URL: http://dx.doi.org/10.1016/j.sedgeo.2013.03.017.

Ezz, H. and J. Imran (2014). "Curvature-induced secondary flow in submarine channels". In: *Environ Fluid Mech* 14.2, pp. 343–370. ISSN: 1573-1510. DOI: 10.1007/s10652-014-9345-4. URL: http://dx.doi.org/10.1007/s10652-014-9345-4.

Gamboa, D., T. M. Alves, and J. Cartwright (2012). "A submarine channel confluence classification for topographically confined slopes". In: *Marine and Petroleum Geology* 35.1, pp. 176–189. ISSN: 0264-8172. DOI: 10.1016/j.marpetgeo.2012.02.011. URL: http://dx.doi.org/10.1016/j.marpetgeo.2012.02.011.

Garcia, M. and G. Parker (1993). "Experiments on the entrainment of sediment into suspension by a dense bottom current". In: *Journal of Geophysical Research* 98.C3, p. 4793. ISSN: 0148-0227. DOI: 10.1029/92jc02404. URL: http://dx.doi.org/10.1029/92JC02404.

Greene, H., N. Maher, and C. Paull (2002). "Physiography of the Monterey Bay National Marine Sanctuary and implications about continental margin development". In: *Marine Geology* 181.1-3, pp. 55–82. ISSN: 0025-3227. DOI: 10.1016/s0025-3227(01)00261-4. URL: http://dx.doi.org/10.1016/S0025-3227(01)00261-4.

Gurram, S. K., K. S. Karki, and W. H. Hager (1997). "Subcritical Junction Flow". In: *J. Hydraul. Eng.* 123.5, pp. 447–455. ISSN: 1943-7900. DOI: 10.1061/(asce)0733-9429(1997)123:5(447). URL: http://dx.doi.org/10.1061/(ASCE)0733-9429(1997)123:5(447).

Hay, A. E. (1987). "Turbidity currents and submarine channel formation in Rupert Inlet, British Columbia: 1. Surge observations". In: *Journal of Geophysical Research* 92.C3, p. 2875. ISSN: 0148-0227. DOI: 10.1029/jc092ic03p02875. URL: http://dx.doi.org/10.1029/JC092iC03p02875.

Hesse, R. (1989). "Drainage systems associated with mid-ocean channels and submarine yazoos: Alternative to submarine fan depositional systems". In: *Geology* 17.12, p. 1148. ISSN: 0091-7613. DOI: 10.1130/0091-7613(1989)017<1148:dsawmo>2.3.co;2. URL: http://dx.doi.org/10.1130/0091-7613(1989)017<1148:DSAWMO>2.3.CO;2.

Hsu, C.-C., W.-J. Lee, and C.-H. Chang (1998). "Subcritical Open-Channel Junction Flow". In: *J. Hydraul. Eng.* 124.8, pp. 847–855. ISSN: 1943-7900. DOI: 10.1061/(asce)0733-9429(1998)124:8(847). URL: http://dx.doi.org/10.1061/(ASCE)0733-9429(1998)124:8(847).

Hsu, C.-C., F.-S. Wu, and W.-J. Lee (1998). "Flow at 90 Equal-Width Open-Channel Junction". In: *J. Hydraul. Eng.* 124.2, pp. 186–191. ISSN: 1943-7900. DOI: `10.1061/(asce)0733-9429(1998)124:2(186)`. URL: `http://dx.doi.org/10.1061/(ASCE)0733-9429(1998)124:2(186)`.

Huang, H., J. Imran, and C. Pirmez (2008). "Numerical Study of Turbidity Currents with Sudden-Release and Sustained-Inflow Mechanisms". In: *J. Hydraul. Eng.* 134.9, pp. 1199–1209. ISSN: 1943-7900. DOI: `10.1061/(asce)0733-9429(2008)134:9(1199)`. URL: `http://dx.doi.org/10.1061/(ASCE)0733-9429(2008)134:9(1199)`.

— (2012). "The depositional characteristics of turbidity currents in submarine sinuous channels". In: *Marine Geology* 329-331, pp. 93–102. ISSN: 0025-3227. DOI: `10.1016/j.margeo.2012.08.003`. URL: `http://dx.doi.org/10.1016/j.margeo.2012.08.003`.

Imran, J., G. Parker, and N. Katopodes (1998). "A numerical model of channel inception on submarine fans". In: *Journal of Geophysical Research* 103.C1, p. 1219. ISSN: 0148-0227. DOI: `10.1029/97jc01721`. URL: `http://dx.doi.org/10.1029/97JC01721`.

Islam, M. A. and J. Imran (2008). "Experimental modeling of gravity underflow in a sinuous submerged channel". In: *Journal of Geophysical Research* 113.C7. ISSN: 0148-0227. DOI: `10.1029/2007jc004292`. URL: `http://dx.doi.org/10.1029/2007JC004292`.

Janocko, M. et al. (2013). "Turbidity current hydraulics and sediment deposition in erodible sinuous channels: Laboratory experiments and numerical simulations". In: *Marine and Petroleum Geology* 41, pp. 222–249. ISSN: 0264-8172. DOI: `10.1016/j.marpetgeo.2012.08.012`. URL: `http://dx.doi.org/10.1016/j.marpetgeo.2012.08.012`.

Keeulegan, G. (1949). "Interfacial instability and mixing in stratified flows". In: *J. Res US Bur Stand* 43, pp. 487–500.

Kesserwani, G. et al. (2008). "Simulation of subcritical flow at open-channel junction". In: *Advances in Water Resources* 31.2, pp. 287–297. ISSN: 0309-1708. DOI: `10.1016/j.advwatres.2007.08.007`. URL: `http://dx.doi.org/10.1016/j.advwatres.2007.08.007`.

Khripounoff, A. et al. (2003). "Direct observation of intense turbidity current activity in the Zaire submarine valley at 4000 m water depth". In: *Marine Geology* 194.3-4, pp. 151–158. ISSN: 0025-3227. DOI: `10.1016/s0025-3227(02)00677-1`. URL: `http://dx.doi.org/10.1016/S0025-3227(02)00677-1`.

41

Klaucke, I., R. Hesse, and W. B. F. Ryan (1998). "Morphology and structure of a distal submarine trunk channel: The northwest Atlantic Mid-Ocean Channel between lat 53 degrees N and 44 degrees 30 ' N". In: *Geological Society of America Bulletin* 110, pp. 22–34.

Kneller, B. and C. Buckee (2000). "The structure and fluid mechanics of turbidity currents: a review of some recent studies and their geological implications". In: *Sedimentology* 47, pp. 62–94. ISSN: 0037-0746. DOI: 10.1046/j.1365-3091.2000.047s1062.x. URL: http://dx.doi.org/10.1046/j.1365-3091.2000.047s1062.x.

Kneller, B. C., S. J. Bennett, and W. D. McCaffrey (1999). "Velocity structure, turbulence and fluid stresses in experimental gravity currents". In: *Journal of Geophysical Research* 104.C3, p. 5381. ISSN: 0148-0227. DOI: 10.1029/1998jc900077. URL: http://dx.doi.org/10.1029/1998JC900077.

Kolla, V., H. Posamentier, and L. Wood (2007). "Deep-water and fluvial sinuous channels–Characteristics, similarities and dissimilarities, and modes of formation". In: *Marine and Petroleum Geology* 24.6-9, pp. 388–405. ISSN: 0264-8172. DOI: 10.1016/j.marpetgeo.2007.01.007. URL: http://dx.doi.org/10.1016/j.marpetgeo.2007.01.007.

L'Heureux, J.-S., L. Hansen, and O. Longva (2009). "Development of the submarine channel in front of the Nidelva River, Trondheimsfjorden, Norway". In: *Marine Geology* 260.1-4, pp. 30–44. ISSN: 0025-3227. DOI: 10.1016/j.margeo.2009.01.005. URL: http://dx.doi.org/10.1016/j.margeo.2009.01.005.

Lin, J. D. and H. K. Soong (1979). "Junction losses in open channel flows". In: *Water Resour. Res.* 15.2, pp. 414–418. ISSN: 0043-1397. DOI: 10.1029/wr015i002p00414. URL: http://dx.doi.org/10.1029/WR015i002p00414.

Mitchell, N. C. (2004). "Form of submarine erosion from confluences in Atlantic USA continental slope Canyons". In: *American Journal of Science* 304.7, pp. 590–611. ISSN: 0002-9599. DOI: 10.2475/ajs.304.7.590. URL: http://dx.doi.org/10.2475/ajs.304.7.590.

Normark, W. R. (1989). "Observed Parameters for Turbidity-Current Flow in Channels, Reserve Fan, Lake Superior". In: *SEPM JSR* Vol. 59. ISSN: 1527-1404. DOI: 10.1306/212f8fb2-2b24-11d7-8648000102c1865d. URL: http://dx.doi.org/10.1306/212F8FB2-2B24-11D7-8648000102C1865D.

Paquet, F. et al. (2010). "Buried fluvial incisions as a record of Middle-Late Miocene eustasy fall on the Armorican Shelf (Bay of Biscay, France)". In: *Marine Geology* 268.1-4, pp. 137–151. ISSN: 0025-3227. DOI: 10.1016/j.margeo.2009.11.002. URL: http://dx.doi.org/10.1016/j.margeo.2009.11.002.

Parker, G. et al. (1987). "Experiments on turbidity currents over an erodible bed". In: *Journal of Hydraulic Research* 25.1, pp. 123–147. ISSN: 1814-2079. DOI: 10.1080/00221688709499292. URL: http://dx.doi.org/10.1080/00221688709499292.

Parker, G., Y. Fukushima, and H. M. Pantin (1986). "Self-accelerating turbidity currents". In: *Journal of Fluid Mechanics* 171.-1, p. 145. ISSN: 1469-7645. DOI: 10.1017/s0022112086001404. URL: http://dx.doi.org/10.1017/S0022112086001404.

Paull, C. K. et al. (2002). "Caught in the act: the 20 December 2001 gravity flow event in Monterey Canyon". In: *Geo-Marine Letters* 22.4, pp. 227–232. ISSN: 1432-1157. DOI: 10.1007/s00367-003-0117-2. URL: http://dx.doi.org/10.1007/s00367-003-0117-2.

Peakall, J., B. McCaffrey, and B. Kneller (2000). "A Process Model for the Evolution, Morphology, and Architecture of Sinuous Submarine Channels". In: *Journal of Sedimentary Research* 70.3, pp. 434–448. ISSN: 1527-1404. DOI: 10.1306/2dc4091c-0e47-11d7-8643000102c1865d. URL: http://dx.doi.org/10.1306/2DC4091C-0E47-11D7-8643000102C1865D.

Peakall, J. et al. (2007). "Flow processes and sedimentation in submarine channel bends". In: *Marine and Petroleum Geology* 24.6-9, pp. 470–486. ISSN: 0264-8172. DOI: 10.1016/j.marpetgeo.2007.01.008. URL: http://dx.doi.org/10.1016/j.marpetgeo.2007.01.008.

Pirmez, C. and J. Imran (2003). "Reconstruction of turbidity currents in Amazon Channel". In: *Marine and Petroleum Geology* 20.6-8, pp. 823–849. ISSN: 0264-8172. DOI: 10.1016/j.marpetgeo.2003.03.005. URL: http://dx.doi.org/10.1016/j.marpetgeo.2003.03.005.

Prior, D. B. et al. (1987). "Turbidity Current Activity in a British Columbia Fjord". In: *Science* 237.4820, pp. 1330–1333. ISSN: 1095-9203. DOI: 10.1126/science.237.4820.1330. URL: http://dx.doi.org/10.1126/science.237.4820.1330.

Qing-Yuan, Y. et al. (2009). "Experimental Study on Characteristics of Separation Zone in Confluence Zones in Rivers". In: *J. Hydrol. Eng.* 14.2, pp. 166–171. ISSN: 1943-5584. DOI: 10.1061/(asce)1084-0699(2009)14:2(166). URL: http://dx.doi.org/10.1061/(ASCE)1084-0699(2009)14:2(166).

Sequeiros, O. E. et al. (2010). "Bedload transport and bed resistance associated with density and turbidity currents". In: *Sedimentology* 57.6, pp. 1463–1490. ISSN: 0037-0746. DOI: 10.1111/j.1365-3091.2010.01152.x. URL: http://dx.doi.org/10.1111/j.1365-3091.2010.01152.x.

Shabayek, S., P. Steffler, and F. E. Hicks (2002). "Dynamic Model for Subcritical Combining Flows in Channel Junctions". In: *J. Hydraul. Eng.* 128.9, pp. 821–

828. ISSN: 1943-7900. DOI: 10.1061/(asce)0733-9429(2002)128:9(821). URL: http://dx.doi.org/10.1061/(ASCE)0733-9429(2002)128:9(821).

Simpson, J. E. and R. E. Britter (1979). "The dynamics of the head of a gravity current advancing over a horizontal surface". In: *Journal of Fluid Mechanics* 94.03, p. 477. ISSN: 1469-7645. DOI: 10.1017/s0022112079001142. URL: http://dx.doi.org/10.1017/S0022112079001142.

Straub, K. M. et al. (2007). "Interactions between turbidity currents and topography in aggrading sinuous submarine channels: A laboratory study". In: *Geological Society of America Bulletin* 120.3-4, pp. 368–385. ISSN: 1943-2674. DOI: 10.1130/b25983.1. URL: http://dx.doi.org/10.1130/B25983.1.

Straub, K. M. et al. (2011). "Quantifying the influence of channel sinuosity on the depositional mechanics of channelized turbidity currents: A laboratory study". In: *Marine and Petroleum Geology* 28.3, pp. 744–760. ISSN: 0264-8172. DOI: 10.1016/j.marpetgeo.2010.05.014. URL: http://dx.doi.org/10.1016/j.marpetgeo.2010.05.014.

Tokyay, T. E. and M. H. Garcia (2013). "Effect of initial excess density and discharge on constant flux gravity currents propagating on a slope". In: *Environ Fluid Mech* 14.2, pp. 409–429. ISSN: 1573-1510. DOI: 10.1007/s10652-013-9317-0. URL: http://dx.doi.org/10.1007/s10652-013-9317-0.

Vachtman, D., N. C. Mitchell, and R. Gawthorpe (2013). "Morphologic signatures in submarine canyons and gullies, central USA Atlantic continental margins". In: *Marine and Petroleum Geology* 41, pp. 250–263. ISSN: 0264-8172. DOI: 10.1016/j.marpetgeo.2012.02.005. URL: http://dx.doi.org/10.1016/j.marpetgeo.2012.02.005.

Vangriesheim, A., A. Khripounoff, and P. Crassous (2009). "Turbidity events observed in situ along the Congo submarine channel". In: *Deep Sea Research Part II: Topical Studies in Oceanography* 56.23, pp. 2208–2222. ISSN: 0967-0645. DOI: 10.1016/j.dsr2.2009.04.004. URL: http://dx.doi.org/10.1016/j.dsr2.2009.04.004.

Webber, N. B. and C. A. Greated (1966). "An investigation of flow behaviour at the junction of rectangular channels." In: *ICE Proceedings* 34.3, pp. 321–334. ISSN: 1753-7789. DOI: 10.1680/iicep.1966.8925. URL: http://dx.doi.org/10.1680/iicep.1966.8925.

Wynn, R. B., B. T. Cronin, and J. Peakall (2007). "Sinuous deep-water channels: Genesis, geometry and architecture". In: *Marine and Petroleum Geology* 24.6-9, pp. 341–387. ISSN: 0264-8172. DOI: 10.1016/j.marpetgeo.2007.06.001. URL: http://dx.doi.org/10.1016/j.marpetgeo.2007.06.001.

44

Xu, J. P., M. A. Noble, and L. K. Rosenfeld (2004). "In-situ measurements of velocity structure within turbidity currents". In: *Geophysical Research Letters* 31.9. ISSN: 0094-8276. DOI: 10.1029/2004gl019718. URL: http://dx.doi.org/10.1029/2004GL019718.